공학석사 학위논문

Effect of Fluorine Substitution on Photovoltaic Performance of DPP-based Copolymer for Polymer Solar Cell

고분자 태양전지에 사용되는

DPP 기반 고분자의 불소 치환이

광전지 성능에 미치는 효과

2015년 2월

서울대학교 대학원

재료공학부

이 진 용

Abstract

Effect of Fluorine Substitution on Photovoltaic Performance of DPP-based Copolymer for Polymer Solar Cell

Lee, Jin Yong

Department of Materials Science and Engineering

Seoul National University

Low bandgap conjugated copolymers composed of thiophene-capped diketopyrrolopyrrole and benzene with/without fluorination were synthesized to investigate the effect of fluorine substitution on their photovoltaic properties. With increasing the number of substituted fluorine atom on benzene, both HOMO and LUMO energy levels of the copolymer are lowered and its crystallinity is increased. The fibril size of copolymer:$PC_{71}BM$ blend becomes smaller as the number of substituted fluorine increases. As a result, the copolymer with two fluorine substitution exhibits deeper HOMO energy level (−5.30 eV), leading to higher V_{OC} (0.72 V), and also enhanced crystallinity (polymer chain packing), leading to higher J_{SC} (12.4 mA cm^{-2}) as compared to mono- and non-fluorinated ones. The copolymer with two fluorine atoms shows a promising power conversion efficiency of 5.63%.

Keywords: polymer solar cell, diketopyrrolopyrrole, conjugated polymer, fluorination

Student Number: 2013-22480

Contents

List of Schemes

List of Figures

List of Tables

1. Introduction

As sources of alternative energy are increasingly recognized to be more important in recent years, solar energy can potentially provide a clean, sustainable alternative to fossil fuels to meet the global growing needs for energy.[1] Polymer solar cells (PSCs) are a promising alternative for producing clean and renewable energy because of the possibility of a production on flexible and large-area substrates by solution processing which should dramatically reduce the manufacturing costs.[2-4] Recent reports of efficiencies approaching and exceeding 10% have continued to draw interest in this research field.[5-9]

A fundamental key to operate PSCs is that light absorption results in the formation of excitons in organic semiconducting materials. Exciton is coulombicly bound electron hole pair and the coulombic binding energy is approximately 0.3 eV. To separate the generated exciton into free charge carriers, exciton should diffuse to the interface between electron-pulling-material (acceptor) and hole-pulling-material (donor). At the interface, the energy offset between the donor and acceptor LUMO energy level is utilized to dissociate excitons.[10-13] Therefore, the most widely utilized device structure of PSCs is bulk heterojunction (BHJ) because optimized BHJ structure has large degree of interlayer contact between donor and acceptor, which helps exciton reach to donor/acceptor interface within its diffusion length. [4, 14]

In past decades, it seemed very difficult to achieve the power conversion efficiency (PCE) for an industrialization of the solar cells. However, the

record high efficiency has continually increased to its current value of higher over 8% due to synergetic advancement in the understanding of the physics of PSCs, device optimization, and development of new materials.[15-17] One of the most successful approaches to achieve high efficiency polymer solar cells is to develop low bandgap conjugated polymers.[18-23] Synthesis of alternating copolymers composed of electron-donating (D) and electron-accepting (A) units has been considered as the most promising method to develop low bandgap polymers, and more importantly this method provides large flexibility in tuning the molecular energy levels of the copolymer.[24-28]

Among various electron-accepting units, diketopyrrolopyrrole (DPP) has attracted much attention because of easy synthesis, high molar absorptivity, highly conjugated structure, strong π–π interaction and strong electron deficiency. Hence, many DPP-based D–A type low bandgap polymers have recently been developed, and the devices fabricated from DPP-based polymers have currently achieved the PCE up to 7%.[29-32] Particularly, broad absorption up to the near-infrared region and high charge carrier mobility are significant features of DPP-based polymers, leading to high short circuit current (J_{SC}) and high fill factor (FF) of PSC device. However, most of DPP-based polymers have exhibited low V_{OC}s due to high-lying highest occupied molecular orbital (HOMO) energy level.[33, 34]

The molecular energy levels of conjugated copolymers depend upon several factors including molecular weight, chain planarity, strength of electron-donating and electron-accepting power in copolymer, and electronic properties of substituent, etc. Among these factors, the substitution of fluorine

atom in conjugated copolymers has recently been a promising method to control the energy levels, because (1) it can lower the HOMO energy level of copolymers, which results in an increased open-circuit voltage (V_{OC}) because V_{OC} is proportional to the difference between the HOMO energy level of donor polymer and the lowest unoccupied molecular orbital (LUMO) energy level of acceptor; [35-37] (2) it facilitates inter/intramolecular interaction due to strong dipole of C–F, which leads to high charge carrier mobility and well-developed fibril structure in active layer of PSCs, contributing to both enhancement of J_{SC} and FF.[38, 39]

Recently, PSCs composed of D–A type polymers with fluorinated electron-donating unit (D) have been reported.[40-42] Li *et al*. introduced fluorine atom on biphenyl unit in DPP-biphenyl copolymer to lower the HOMO and LUMO energy levels. As a result, a medium bandgap (1.70 eV) DPP-polymer affords a high V_{OC} of 0.93 V and a PCE of 4.1% in solar cells with $PC_{71}BM$.[40] Very recently, Jo *et al*. reported the effect of fluorination on photophysical properties of conjugated copolymers and their photovoltaic performances, suggesting that fluorination on D unit in D–A type conjugated copolymer is a promising method to achieve high performance solar cells.[41, 42]

In this work, we synthesized low bandgap conjugated polymers composed of DPP as electron-accepting (A) unit and benzene with/without fluorination as electron-donating (D) unit to examine the effect of the number of substituted fluorine on their photovoltaic properties. The copolymers with fluorinated benzene exhibit higher V_{OC}s due to deeper HOMO energy levels than the copolymer with non-fluorinated benzene and also higher J_{SC}s due to

enhanced molecular ordering. The copolymer with two fluorine atom substitution exhibits the highest PCE of 5.63% with a V_{OC} of 0.72 V and a J_{SC} of 12.4 mA cm^{-2}, which are higher than the values of copolymers with mono- and non-substituted fluorine.

2. Experimental Section

2.1. Materials

All reagents and solvents were purchased from Sigma-Aldrich, TCI and Acros, and used without further purification. [6,6]-Phenyl-C_{71}-butyric acid methyl ester ($PC_{71}BM$) was obtained from American Dye Source. Poly(3,4-ethylenedioxy-thiophene):poly(styrene sulfonate) (PEDOT:PSS) (Clevios P VP AI 4083) was purchased from H. C. Stark and passed through a 0.45 m PVDF syringe filter before spin-coating.

2.2. Synthesis of monomers

2.2.1. Synthesis of 3,6-di(thien-2-yl)pyrrolo[3,4-c]pyrrole-1,4(2H, 5H)-dione (1)

A 500 mL three-neck flask connected to a condenser was charged with a stir bar and tert-amyl alcohol (250 mL). Sodium metal (2.56 g, 108 mmol) immersed in mineral oil was thoroughly washed with hexanes and cut into small pieces. The sodium metal pieces were slowly added to the reaction mixture over a 1.5 h period while the temperature was slowly increased to 120 ℃. After all the sodium metal pieces were dissolved, thiophene-2-corbonitrile (11.9 g, 108 mmol) was added to the reaction. As dimethyl succinate (5.29 g, 36.2 mmol) was added dropwise to the reaction mixture over 1 h, the solution turned dark red. The reaction contents were stirred at 120 ℃ for 2 h, and then precipitated into acidic MeOH (400 mL MeOH and 20 mL conc. HCl). Filtration of the suspension through a Buchner funnel

yielded the product as a dark red solid (9.10 g, 83%). This product was used in subsequent reactions without further purification. ^{1}H NMR (300 MHz, $CDCl_3$): δ (ppm) 11.20 (s, 2H), 8.14 (d, 2H), 7.90 (d, 2H), 7.23 (t, 2H). m/z (MS-EI) calcd: 300, found: 300.

2.2.2. Synthesis of 2,5-bis(2-decyltetradecyl)-3,6-di(thiophen-2-yl)pyrrolo[3,4-c]pyrrole-1,4(2H,5H)-dione (2)

In a dry three-neck 250 mL round bottom flask was charged with **1** (7.0 g, 23.3 mmol), and K_2CO_3 (9.0 g, 69.9 mmol) were dissolved in anhydrous *N*,*N*-dimethylformamide (DMF) (250 mL), and heated to 120 ℃ under argon for 1 h. And then 2-2-decyltetradecyl bromide (17.74 g, 58.3 mmol) was added drop-wise, and the reaction mixture was further stirred and heated overnight at 130 ℃. The reaction mixture was allowed to cool down to room temperature, poured into water, and stirred for 30 min. The product was extracted with chloroform, then washed with water, and dried over magnesium sulfate. Removal of the solvent afforded the crude product which was further purified using column chromatography on silica gel using a mixture of hexane and chloroform as eluent, giving the product as a purple solid. (11.0g, 53.5%). ^{1}H NMR (300 MHz, $CDCl_3$): δ (ppm) 8.88 (d, 2H), 7.62 (d, 2H), 7.27 (d, 2H), 4.03 (d, 4H), 1.91 (m, 2H), 1.30–1.21 (m, 80H), 0.89–0.87 (m, 12H). m/z (MS-EI) calcd: 972, found: 972.

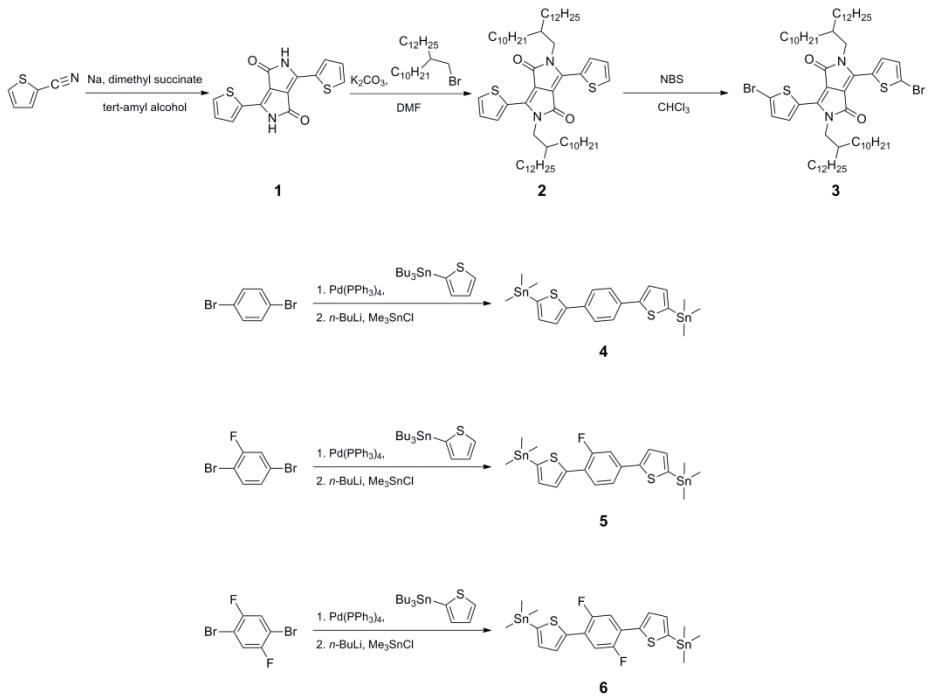

Scheme 2.1 The whole synthetic route of monomers

2.2.3. Synthesis of 3,6-bis(5-bromothiophen-2-yl)-2,5-bis(2-decyltetradecyl)pyrrolo[3,4-c]pyrrole-1,4(2H,5H)-dione (3)

N-bromosuccininide (1.26g, 7.08 mmol) was added slowly to a solution of the compound **2** (3g, 3.08mmol) in $CHCl_3$ (100mL). The solution was protected from light and stirred at room temperature for 48 h. The reaction mixture was poured into water (100 mL) and extracted with $CHCl_3$. The organic layer was dried over magnesium sulfate and the solvent was evaporated under reduced pressure. Purification by flash chromatography (20 % hexanes in $CHCl_3$) yielded a purple solid (1.7g, 52 %). ^{1}H NMR (300 MHz, $CDCl_3$): δ (ppm) 8.63 (d, 2H), 7.22 (d, 2H), 7.52 (d, 2H), 3.98 (d, 4H), 1.88 (s, 2H), 1.30–1.21 (m, 80H), 0.89–0.87 (m, 12H). m/z (MS-EI) calcd: 1128, found: 1128.

2.2.4. Synthesis of 1,4-bis(5-(trimethylstannyl)thiophen-2-yl) benzene (4)

Tetrakis(triphenylphosphine)palladium(0) (140 mg, 0.21 mmol) was added to a solution of 1,4-dibromobenzene (2.00 g, 8.48 mmol) and 2-(tributylstannyl)thiophene (6.49 g, 17.38 mmol) in toluene (30 mL) at room temperature under an argon atmosphere. The mixture was refluxed for 24 h and cooled to room temperature. The reaction mixture was purified using silica gel chromatography. The product was obtained as pure crystals (1.81 g, 88%) by recrystallization from acetone. To the product (1.81 g, 7.47 mmol) in anhydrous THF (30 mL) at −78 ℃, 2.5 M of *n*-BuLi in hexane (6.4 mL, 16.4 mmol) was added dropwise for 30 min. Then, the solution was further

stirred for 30 min at room temperature. The solution was cooled to −78 ℃ again before 1.0 M of trimethyltin chloride in THF (16 mL, 16.4 mmol) was added. After warming up to room temperature and stirring overnight, the resulting mixture was poured into water and extracted with diethyl ether. The organic phase was collected and dried over $MgSO_4$. The final product was purified by recrystallization from acetone to yield the compound **4** as a green solid (2.5 g, 59%). ^{1}H NMR (300 MHz, $CDCl_3$): δ (ppm) 7.60 (s, 4H), 7.41 (m, 2H), 7.17 (m, 2H), 0.39 (m, 18H). m/z (MS-EI) calcd: 568, found: 568.

2.2.5. Synthesis of (5,5'-(2-fluoro-1,4-phenylene)bis(thiophene-5,2-diyl))bis(trimethyl-stannane) (5)

Following the same synthetic procedure as the compound **4** described above, 1.00 g of 1,4-dibromo-2-fluorobenzene, 3.09 g of 2-(tributylstannyl) thiophene, 3.2 mL of *n*-BuLi (2.5 M in hexane), 8.0 mL of trimethyltin chloride (1.0 M in THF) are used to synthesize the compound **5**. The product was obtained as light blue solid (1.2 g, 59%). ^{1}H NMR (300 MHz, $CDCl_3$): δ (ppm) 7.59 (m, 2H), 7.39 (m, 3H), 7.16 (m, 2H), 0.39 (m, 18H). m/z (MS-EI) calcd: 586, found: 586.

2.2.6. Synthesis of (5,5'-(2,5-difluoro-1,4-phenylene)bis(thiophene-5,2-diyl))bis(trimethyl- stannane) (6)

Following the same synthetic procedure as the compound **4** described above, 0.60 g of 1,4-dibromo-2,5-difluorobenzene, 1.73 g of 2-(tributylstannyl) thiophene, 1.6 mL of *n*-BuLi (2.5 M in hexane), 4.0 mL of trimethyltin

chloride (1.0 M in THF) are used to yield the compound **6** as deep blue solid (0.6 g, 58%). ^{1}H NMR (300 MHz, $CDCl_3$): δ (ppm) 7.60 (d, 2H), 7.40(m, 2H), 7.21 (m, 2H), 0.40 (m, 18H). m/z (MS-EI) calcd: 604, found: 604.

2.3. Synthesis of polymers

2.3.1. Synthesis of pPhDPP

1,4-Bis(5-(trimethylstannyl)thiophen-2-yl)benzene (59 mg, 0.1 mmol) and 3,6-bis(5-bromo-2-thienyl)-2,5-dihydro-2,5-di(2´-decyltetradecyl)-pyrrolo[3,4c]pyrrolo-1,4-dione (117 mg, 0.1 mmol) were dissolved in a mixed solvent of toluene (10 mL) and DMF (1 mL). After the solution was flushed with N2 for 20 min, tris(dibenzylideneacetone)dipalladium(0) (4.74 mg, 5.15 μmol) and tri(o-tolyl)phosphine (3.14 mg, 10.30 μmol) were added. The reaction mixture was stirred for 5 h at 150 ℃ in a microwave reactor, followed by end-capping using 2-bromothiophene and 2-tributyltinthiophene. After cooled to room temperature, the mixture was poured into methanol. The crude product was filtered through a Soxhlet thimble and then subjected to Soxhlet extraction successively with methanol, acetone, ethyl acetate, hexane, and chloroform. The polymer was recovered from chloroform fraction, and the fraction was precipitated into acetone to afford the product (pPhDPP) as a dark purple solid (100 mg, 40%). M_n = 98.9 kDa, M_w = 141.1 kDa, PDI = 1.43 ^{1}H NMR (500 MHz, $CDCl_3$): δ (ppm) 8.93–8.61 (m, 2H), 7.62–7.55 (m, 6H), 7.11–7.04 (m, 4H), 3.97 (d, 4H), 1.94 (s, 2H), 1.25–0.85 (br, 92H).

2.3.2. Synthesis of p1FPhDPP

Following the same procedure as pPhDPP described above, 64 mg of (5,5'-(2-fluoro-1,4-phenylene)bis(thiophene-5,2-diyl))bis(trimethylstannane) and 123 mg of 3,6-bis(5-bromo-2-thienyl)-2,5-dihydro-2,5-di(2´-decyltetradecyl)-pyrrolo[3,4c]pyrrolo-1,4-dione are used to afford the product (p1FPhDPP) as a dark purple solid (125 mg, 47%). M_n = 126.1 kDa, M_w = 172.4 kDa, PDI = 1.37 ^{1}H NMR (500 MHz, $CDCl_3$): δ (ppm) 9.10–8.72 (m, 2H), 7.51–7.35 (m, 5H), 7.19–7.04 (m, 4H), 3.96 (d, 4H), 1.94 (s, 2H), 1.25–0.85 (br, 92H).

2.3.3. Synthesis of p2FPhDPP

Following the same procedure as pPhDPP described above, 67 mg of (5,5'-(2,5-difluoro-1,4-phenylene)bis(thiophene-5,2-diyl))bis(trimethylstannane) and 125 mg of 3,6-bis(5-bromo-2-thienyl)-2,5-dihydro-2,5-di(2´-decyltetradecyl)-pyrrolo[3,4c]pyrrolo-1,4-dione are used to afford the product (p2FPhDPP) as a dark purple solid (140 mg, 51%). M_n = 127.2 kDa, M_w = 178.3 kDa, PDI = 1.40 ^{1}H NMR (500 MHz, $CDCl_3$): δ (ppm) 9.01–8.93 (m, 2H), 7.42–7.35 (m, 4H), 7.15–7.04 (m, 4H), 4.00 (d, 4H), 1.94 (s, 2H), 1.25–0.85 (br, 92H).

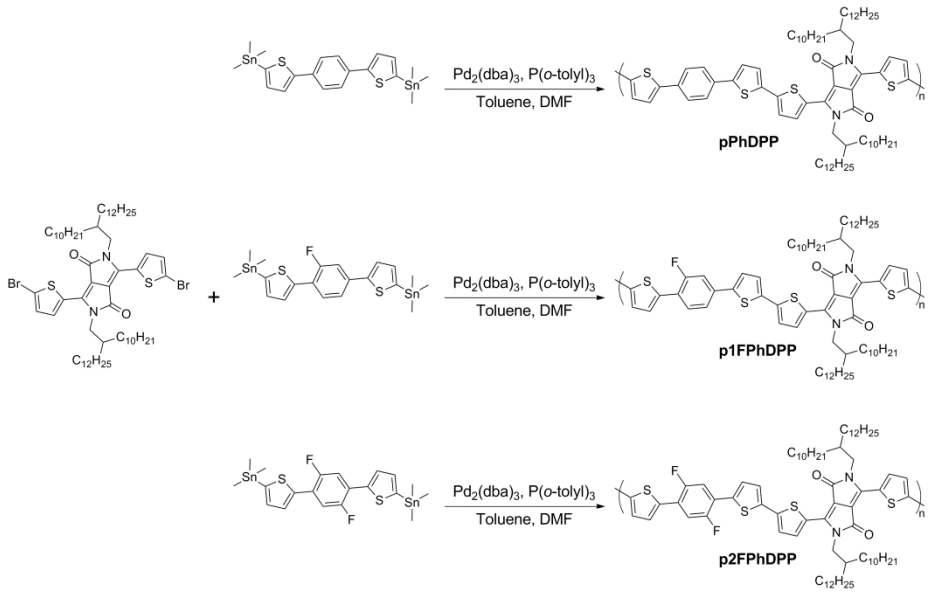

Scheme 2.2 The synthetic scheme of polymers

2.4. Characterization

The chemical structures of compounds were identified by ^{1}H NMR (Avance DPX-300) using d-chloroform ($CDCl_3$) as solvent and tetramethylsilane (TMS) as internal reference. High resolution mass spectrometry (HRMS) analysis was performed on a double focusing mass spectrometer (resolution 60,000, m/z range at full sensitivity 2,400) to measure accurately molar masses of compounds. Thermogravimetric analysis (TGA) were performed on a TA modulated TGA 2050 at a heating rate of 10 ℃ min^{-1} under nitrogen. Molecular weight of polymer and its distribution were measured by gel permeation chromatography (GPC) (Polymer Labs GPC 220) using $CHCl_3$ as an eluent. The optical absorption spectra were obtained by a UV−Vis spectrophotometer (Shimadzu UV-3600). Electrochemical cyclic voltammetry (CV) were conducted on a potentiostat/galvanostat (VMP 3, Biologic) in an electrolyte solution of 0.1 M tetrabutylammonium hexafluorophosphate acetonitrile. Pt wires (Bioanalytical System Inc.) were used as both counter and working electrodes, and silver/silver ion (Ag in 0.1 M $AgNO_3$ solution, Bioanalytical System Inc.) was used as a reference electrode. The HOMO energy levels of polymers were calculated by using the equation: HOMO (eV) = $-[E_{ox} - E_{1/2}(\text{ferrocene}) + 4.8]$, where E_{ox} is the onset oxidation potential of the polymer and $E_{1/2}$(ferrocene) is the onset oxidation potential of ferrocene *vs*. Ag/Ag^+. The crystallinity of polymer was measured by a X-ray diffractometer (M18XHF-SRA, Mac Science Co.) using Cu K_α (λ = 0.154 nm) radiation. The optimized geometries of compounds were obtained by the density functional theory (DFT) calculation at the B3LYP/6-31G(d,p) level using Gaussian 09

software. Thickness of the active layer was measured by an atomic force microscope (Nano Xpert2).

2.5. Device fabrication and measurements

2.5.1. Materials

ITO-patterned glass was used as an anode in PSC device. The sheet resistance of the ITO was less than 10 Ω/square. $PC_{71}BM$ were obtained from Nano-C and used as received. PEDOT:PSS (Clevios P VP AI 4083) was purchased from H.C. Stark and passed through a 0.45 μm PVDF syringe filter before spin-coating.

2.5.2. Fabrication and characterization of photovoltaic cells

The polymer solar cells were fabricated with a conventional configuration of glass/ITO/PEDOT:PSS/polymer:$PC_{71}BM$/Ca/Al (Figure 2.1). Prior to device fabrication, the ITO-coated glass was cleaned with acetone and then isopropyl alcohol for 30 min. After complete drying, the ITO-coated glass was treated with UV–ozone for 20 min. A thin layer of PEDOT:PSS was spin-coated with 40 nm thickness on the ITO-coated glass and annealed at 150 ℃ for 30 min. A 2 wt% solution of polymer:$PC_{71}BM$ blend was dissolved in *o*-dichlorobenzene or *o*-dichlorobenzene with 1-chloronaphtalene (CN) as an additive. The solution was stirred at 110 ℃ for 6 h and spin-coated on the top of PEDOT:PSS at 1000 rpm for 30 s. Calcium (25 nm) and aluminum (100 nm) was thermally evaporated on the top of the active layer under vacuum (< 10^{-6} Torr). The effective area of cell was ca. 0.06 mm^2. The current density–

voltage (*J*–*V*) characteristics were measured with a Keithley 2400 source-meter under AM 1.5G (100 mW/cm^2) simulated by a Newport-Oriel solar simulator. The light intensity was calibrated using a NREL-certified photodiode and a light source meter prior to each measurement. The external quantum efficiency was measured using a lock-in amplifier with a current preamplifier under short circuit current state with illumination of monochromatic light. The space charge limited current (SCLC) *J*–*V* curves were obtained in the dark using hole-only devices (glass/ITO/PEDOT:PSS/polymer:$PC_{71}BM$/Au), and hole mobilities were calculated using the Mott-Gurney square law, $J = (9/8)\varepsilon_0\varepsilon_r\mu(V^2/L^3)$, where ε_0 is vacuum permittivity, ε_r is the dielectric constant of polymer, μ is the charge carrier mobility, V is the effective applied voltage, and L is the thickness of the film. The morphologies of polymer:$PC_{71}BM$ blends were observed by a transmission electron microscope (TEM) (JEOL 2000 FX MARK II) operating at 80 kV of acceleration voltage.

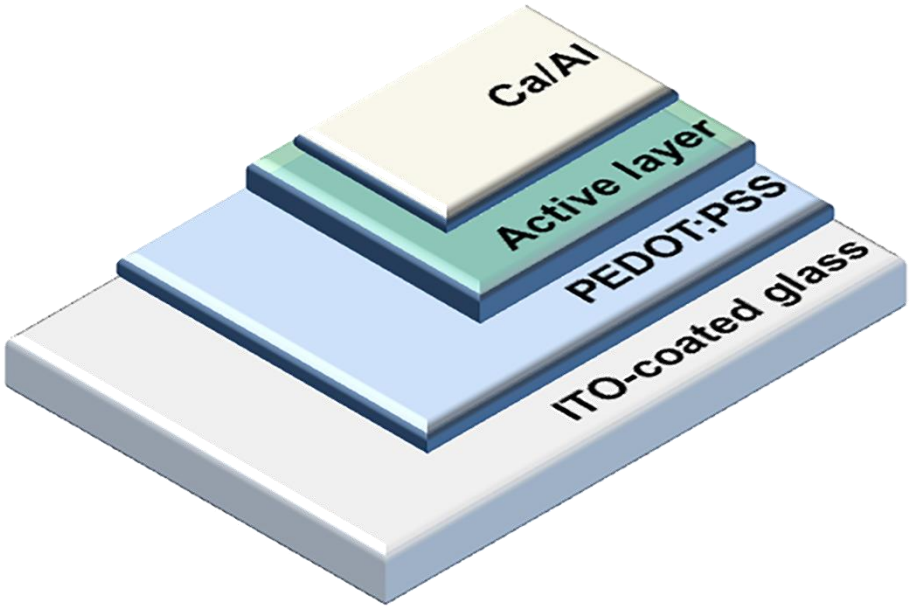

Figure 2.1 Schematic illustration of general structure of PSC device.

3. Results and Discussion

3.1. Synthesis and Characterization

The whole synthetic routes for preparation of the monomers are shown in Scheme 2.1. Three polymers, pPhDPP, p1FPhDPP and p2FPhDPP, were synthesized *via* the Stille coupling reaction in toluene/DMF with $Pd_2(dba)_3$ as a catalyst, as shown in Scheme 2.2. The chemical structures of 3,6-di(thien-2-yl)pyrrolo[3,4-c]pyrrole-1,4(2H, 5H)-dione (1), 2,5-bis(2-decyl-tetradecyl)-3,6-di(thiophen-2-yl)pyrrolo[3,4-c]pyrrole-1,4(2H,5H)-dione (2), 3,6-bis(5-bromothiophen-2-yl)-2,5-bis(2-decyltetradecyl)pyrrolo[3,4-c] pyrrole-1,4(2H, 5H)-dione (3), 1,4-bis(5-(trimethylstannyl)thiophen-2-yl) benzene (4), (5,5'-(2-fluoro-1,4-phenylene)bis(thiophene-5,2-diyl))bis (trimethyl-stannane) (5), (5,5'-(2,5-difluoro-1,4-phenylene)bis(thiophene-5,2-diyl))bis(trimethyl- stannane) (6) are identified by ^{1}H NMR, as shown in Figure 3.1–9, respectively. The molecular weights (M_n) of pPhDPP, p1FPhDPP and p2FPhDPP are 98.9 kDa, 126.1 kDa and 127.2 kDa with polydispersity indexes (PDI) of 1.43, 1.37 and 1.40, respectively, as measured by GPC, as shown in Figure 3.10–12 and listed in Table 3.1. When thermal stability of copolymer was measured by TGA under nitrogen atmosphere, the onset temperatures at 5% weight-loss of all three polymers were nearly the same (412 ℃) (Figure 3.13), indicating that the polymers is thermally stable for its application to PSCs.

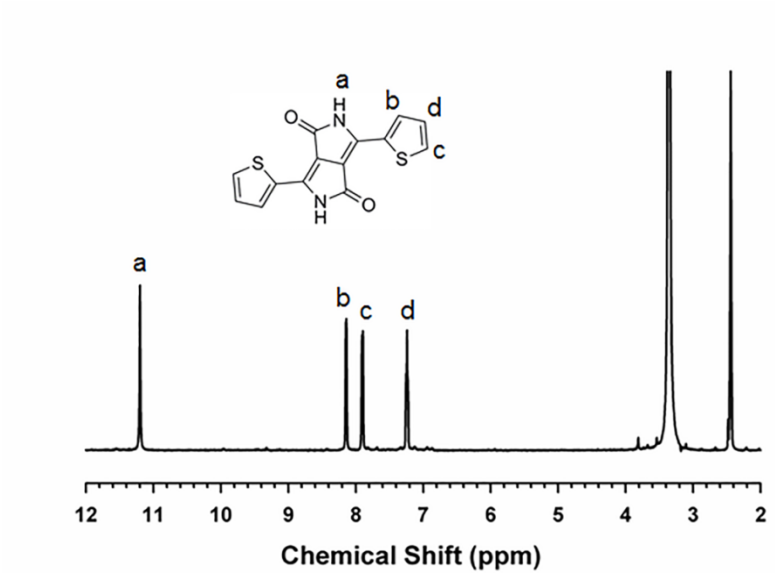

Figure 3.1 Chemical structure and ^{1}H NMR spectrum of 3,6-di(thien-2-yl)pyrrolo[3,4-c]pyrrole-1,4(2H, 5H)-dione.

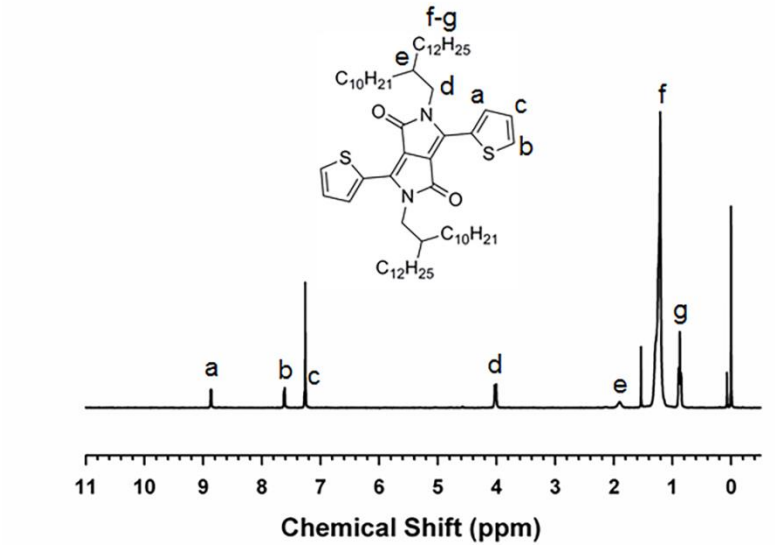

Figure 3.2 Chemical structure and ^{1}H NMR spectrum of 2,5-bis(2-decyl-tetradecyl)-3,6-di(thiophen-2-yl)pyrrolo[3,4-c]pyrrole-1,4(2H,5H)-dione.

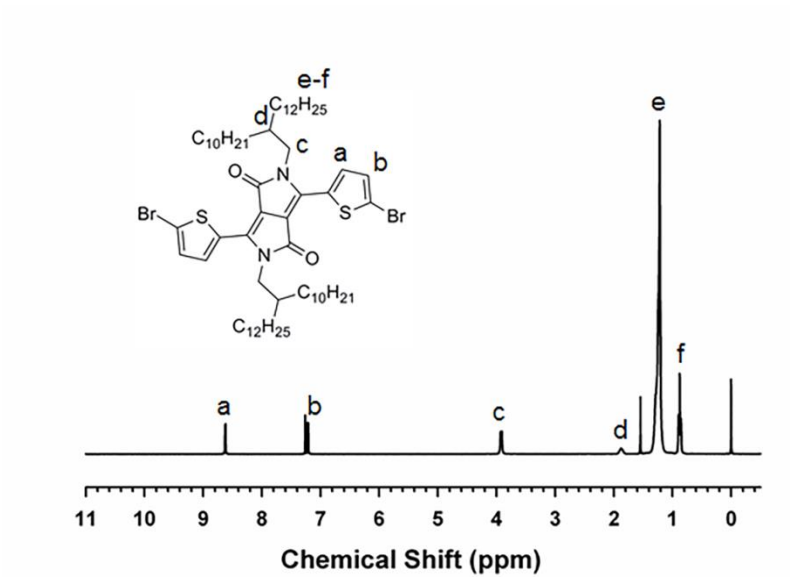

Figure 3.3 Chemical structure and ^{1}H NMR spectrum of 3,6-bis(5-bromothiophen-2-yl)-2,5-bis(2-decyltetradecyl)pyrrolo[3,4-c]pyrrole-1,4 (2H,5H)-dione.

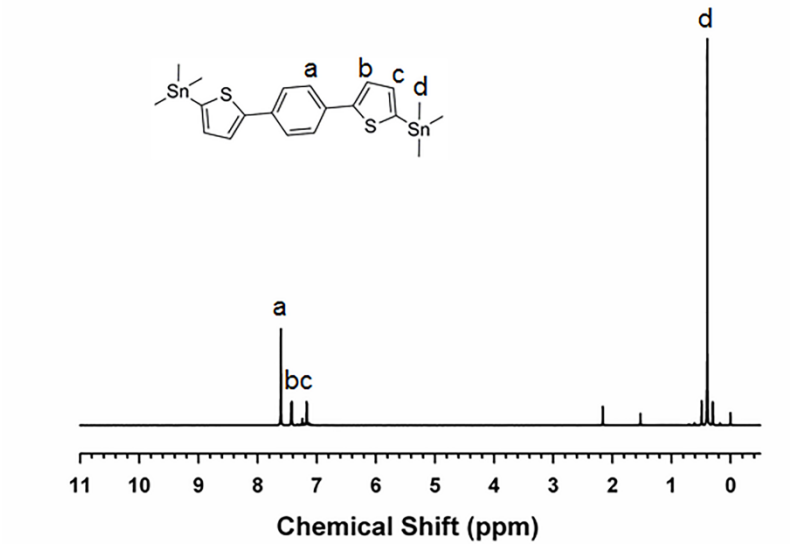

Figure 3.4 Chemical structure and ^{1}H NMR spectrum of 1,4-bis(5-(trimethylstannyl)thiophen-2-yl) benzene.

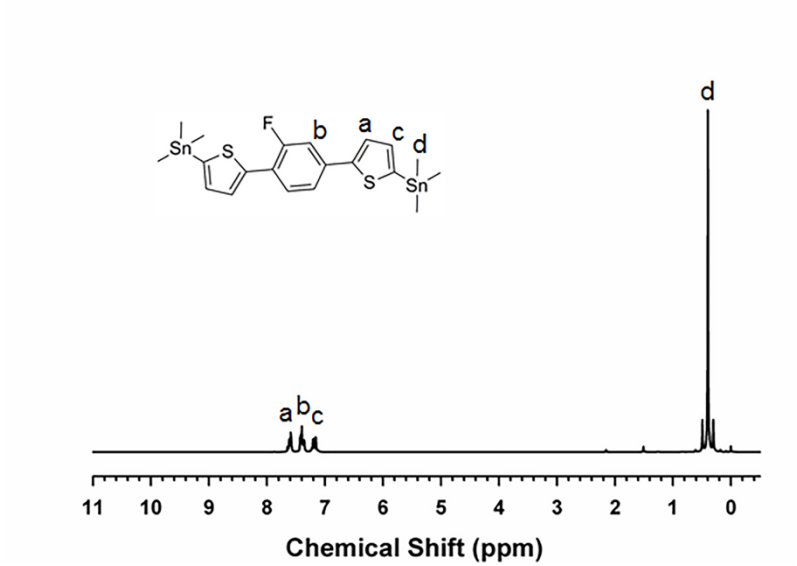

Figure 3.5 Chemical structure and ^{1}H NMR spectrum of (5,5'-(2-fluoro-1,4-phenylene)bis(thiophene-5,2-diyl))bis(trimethyl-stannane).

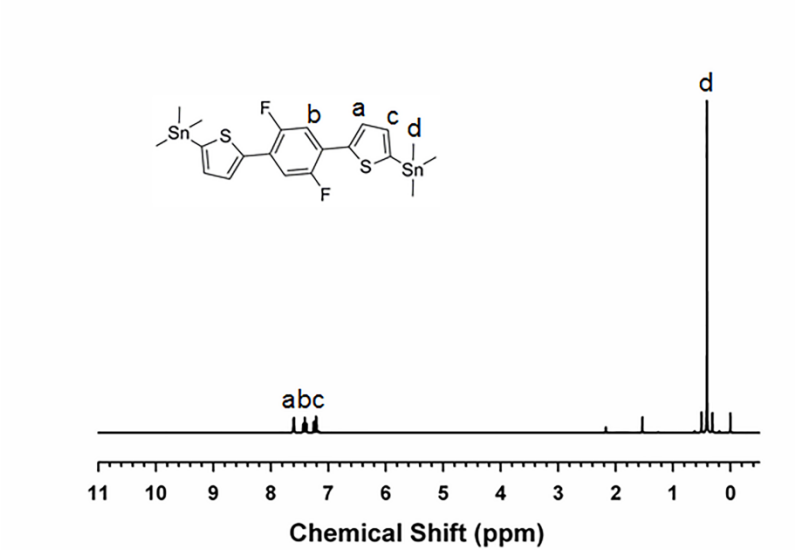

Figure 3.6 Chemical structure and ^{1}H NMR spectrum of (5,5'-(2,5-difluoro-1,4-phenylene)bis(thiophene-5,2-diyl))bis(trimethyl-stannane).

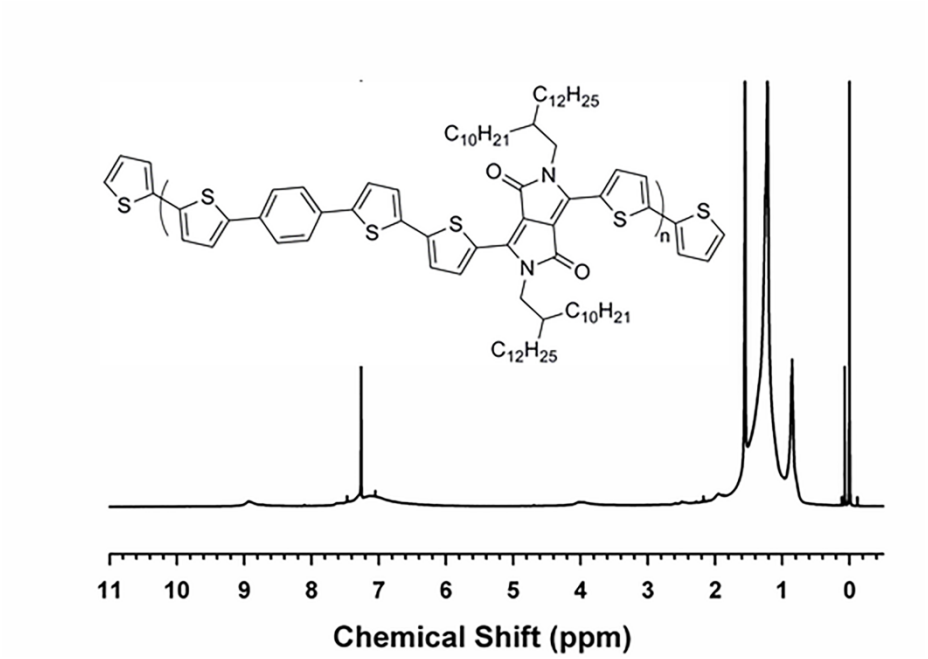

Figure 3.7 Chemical structure and ^{1}H NMR spectrum of pPhDPP.

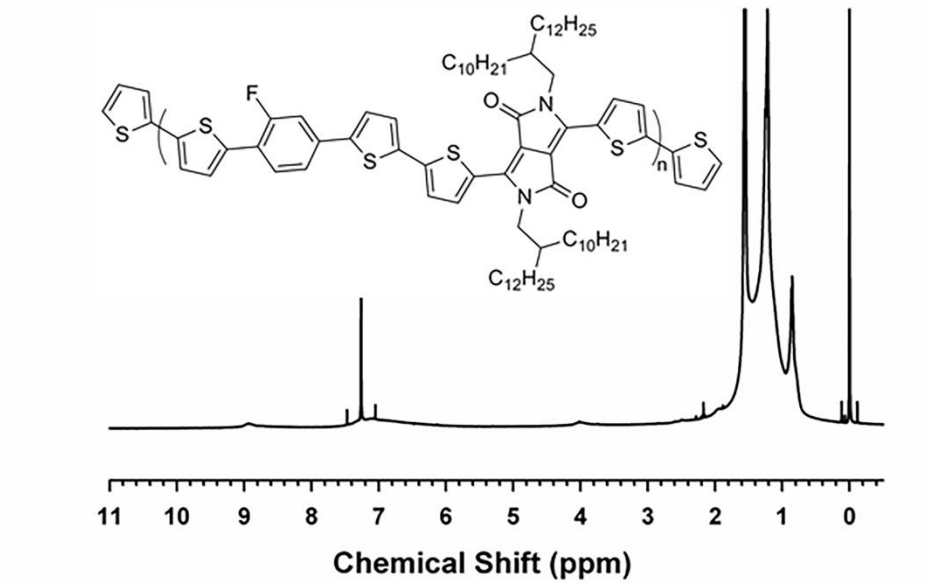

Figure 3.8 Chemical structure and ^{1}H NMR spectrum of p1FPhDPP.

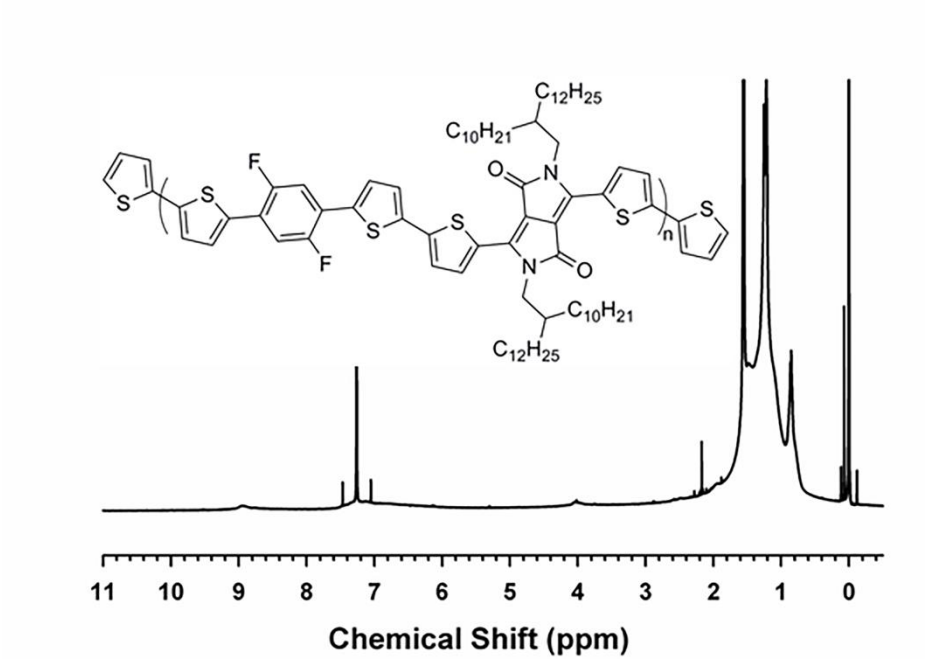

Figure 3.9 Chemical structure and ^{1}H NMR spectrum of p2FPhDPP.

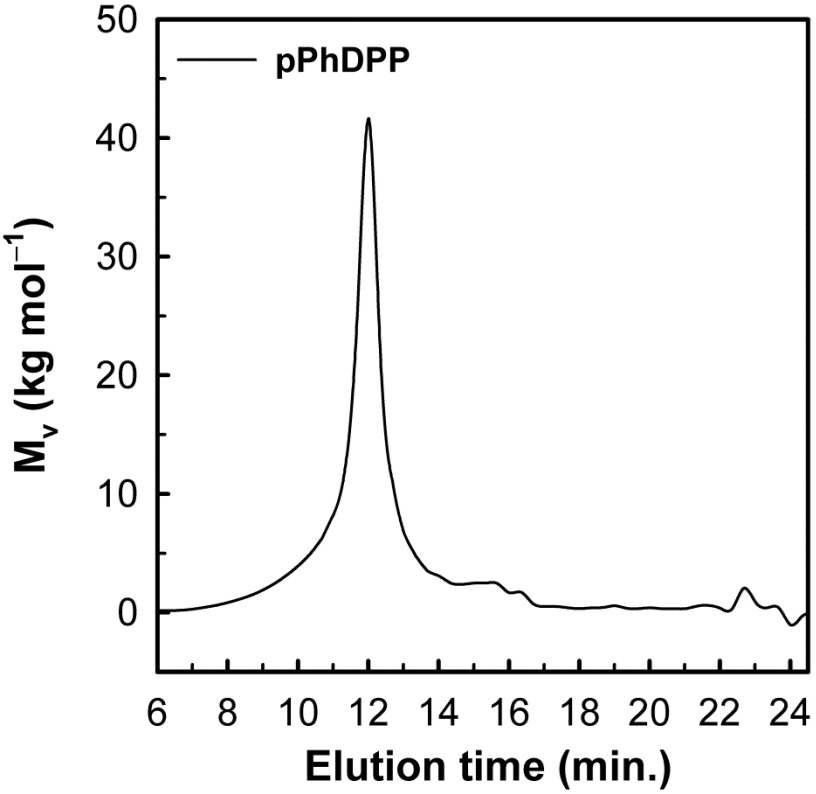

Figure 3.10 GPC trace of pPhDPP eluted with CF (reference: polystyrene).

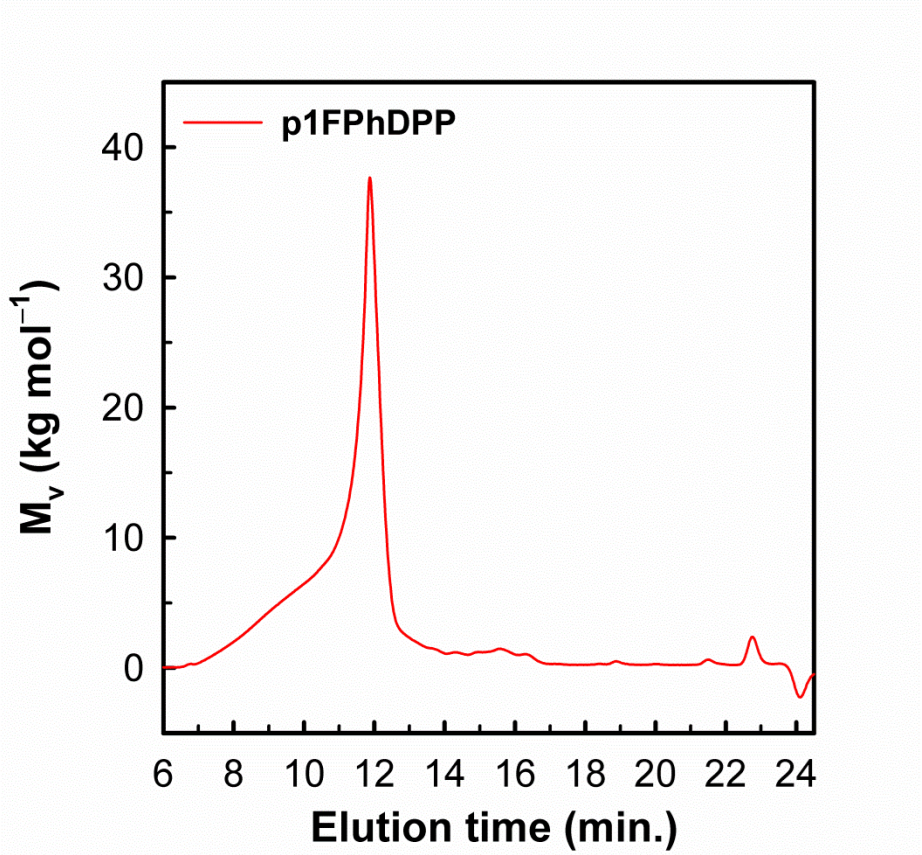

Figure 3.11 GPC trace of p1FPhDPP eluted with CF (reference: polystyrene).

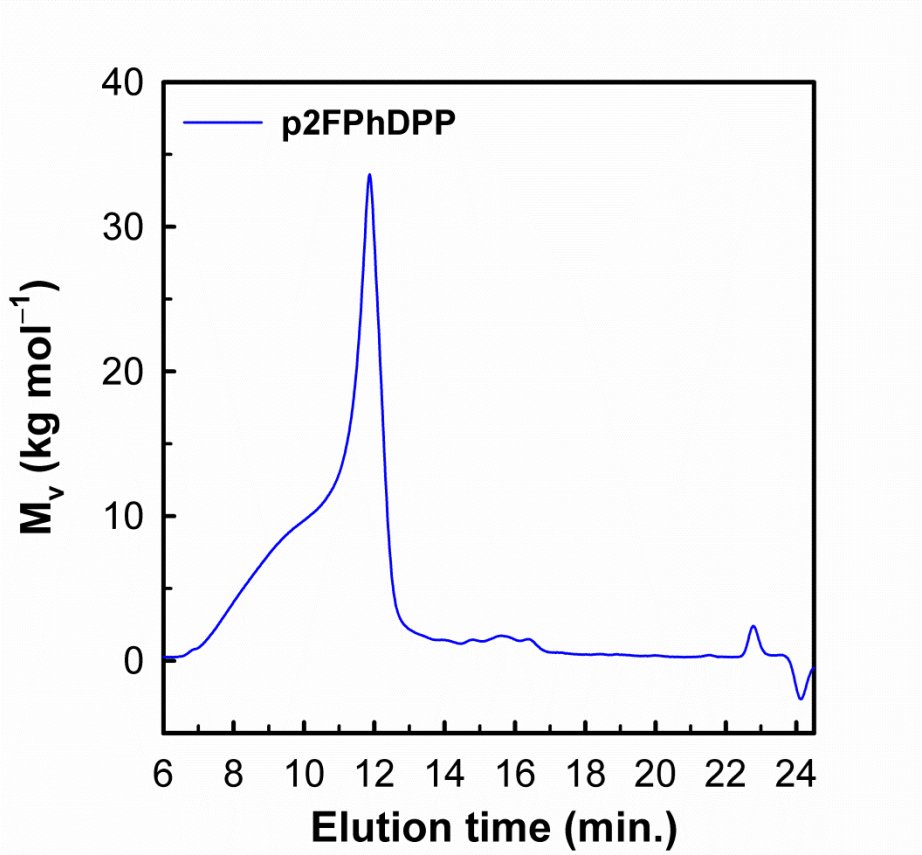

Figure 3.12 GPC trace of p2FPhDPP eluted with CF (reference: polystyrene).

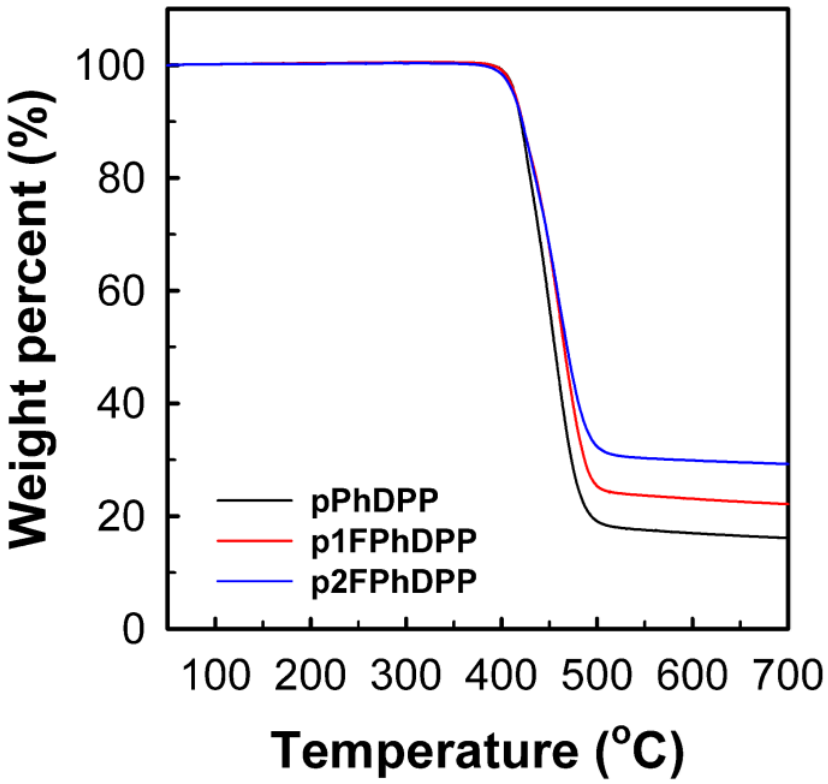

Figure 3.13 TGA thermograms of polymers at a heating rate of 10 ℃ min^{-1} under nitrogen.

3.2. Optical properties

The UV–Vis absorption spectra of polymers in chloroform solution and thin film are shown in Figure 3.14. When the optical bandgap of polymer was determined from the absorption edge of polymer film, three polymers have similar optical bandgap (1.41 ~ 1.48 eV), as listed in Table 3.1. The three polymers pPhDPP, p1FPhDPP and p2FPhDPP showed similar absorption maximums (λ_{max}) at 718 nm, 738 nm, and 742 nm, with a full-width-at-half-maximum (FWHM) of 200 nm, 200 nm, and 213 nm in solution, respectively. In thin film state, λ_{max} of pPhDPP, p1FPhDPP and p2FPhDPP located at 674 nm, 682 nm, and 693 nm, respectively. The FWHM of pPhDPP, p1FPhDPP and p2FPhDPP in the film was 217 nm, 220 nm, and 254 nm, respectively. This broader absorption in film indicates its slightly stronger light-harvesting ability, which is an important factor affecting the current density of PSCs. In both the solution and the film state, the maximum absorption peaks of fluorinated polymers are red-shifted compared to that of non-fluorinated polymer, probably because the fluorine substitution enhances interaction between polymer chains, which may increase the effective conjugation length.[43] It is also noteworthy that two fluorinated polymers (p1FPhDPP and p2FPhDPP) show higher absorptivity and stronger vibronic shoulder at 770 nm than non-fluorinated polymer (pPhDPP) because of enhanced π–π stacking of fluorinated polymer chains, which may contribute to an increase of J_{SC}.

3.3. Electrochemical properties

The electrochemical data of the polymer is obtained from the oxidation and reduction cyclic voltamograms. The HOMO energy level of the polymer was calculated using the equation: HOMO = $-[E_{ox} - E_{1/2}(\text{ferrocene}) + 4.8]$ V, where $E_{1/2}$(ferrocene) and E_{ox} is the onset oxidation potential of ferrocene and polymer *vs*. Ag/Ag^{+} respectively. When the electrochemical properties of polymers were measured from electrochemical cyclic voltammetry, as shown in Figure 3.15 and listed in Table 3.1, the HOMO energy levels of pPhDPP, p1FPhDPP and p2FPhDPP were –5.20 eV, –5.27 eV and –5.30 eV, respectively. The lower HOMO energy levels of fluorinated polymers arise from weaker electron-donating unit due to fluorine substitution on benzene in the polymer. The LUMO energy level of the polymer was calculated from the HOMO energy level and the optical bandgap: LUMO = HOMO + E_g^{opt}. The LUMO energy level of pPhDPP, p1FPhDPP and p2FPhDPP were –3.72 eV, –3.83 eV and –3.89 eV, respectively. Since the open circuit voltage (V_{OC}) of polymer is linearly dependent on the difference between the HOMO energy level of the electron donor and the LUMO energy level of the electron acceptor, the deep HOMO energy level of the donor polymer is expected to afford high V_{OC} for the resulting polymer solar cells. Accordingly, the device fabricated from fluorinated polymer is expected to exhibit higher V_{OC} than the device from non-fluorinated one.

3.4. Structural properties

Geometry optimization of fluorinated donating unit and non-fluorinated donating unit was performed by the DFT calculation to further understand the effect of fluorination on conjugated semiconducting polymer, as shown in Figure 3.16. In the optimized geometries of thiophene-benzene-thiophene, the dihedral angles between thiophene and benzene are 24.9°, 13.4° (22.3°) and 6.2° for Ph (non-fluorinated), 1FPh (one fluorine atom substitution) and 2FPh (two fluorine atoms substitution), respectively, indicating that fluorine substitution leads to coplanar structure.

When X-ray diffraction (XRD) patterns of three polymers are compared to examine the effect of fluorination on molecular packing of polymer chains, as shown in Figure 3.17, the XRD pattern of p2FPhDPP exhibits (010) peak corresponding to π–π stacking distance of 3.70 Å while the patterns of pPhDPP and p1FPhDPP do not show a discernible (010) peak, indicating that fluorination makes polymer backbone more planar, leading to effective stacking of polymer chains in π–π direction.[44]

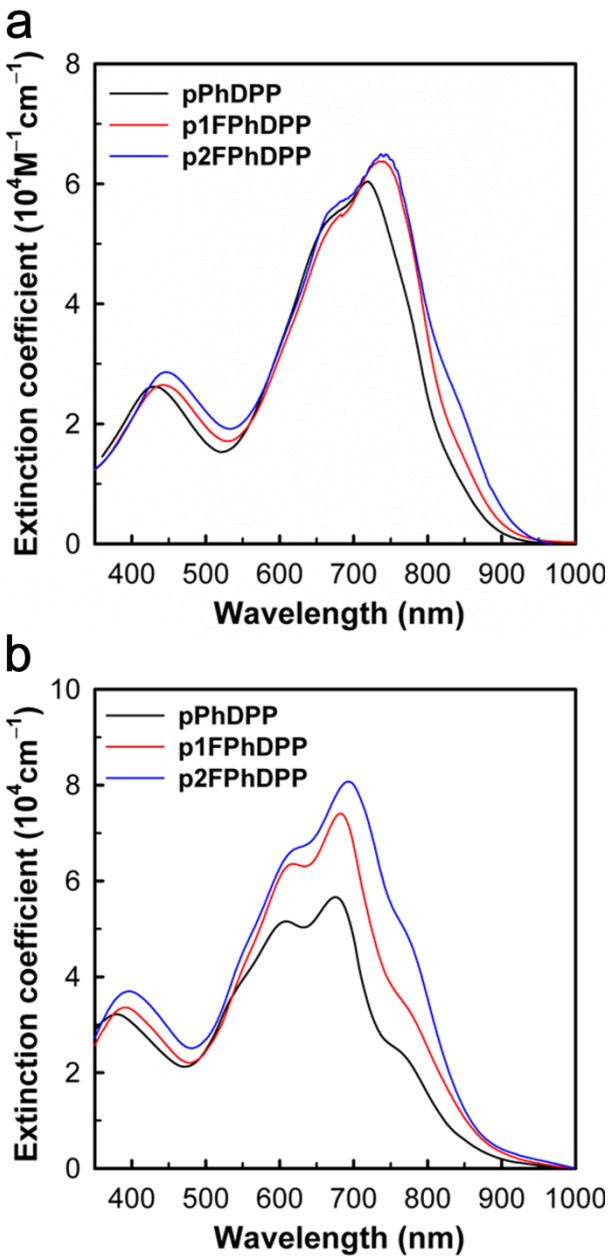

Figure 3.14 UV−Vis absorption spectra of the polymers in (a) $CHCl_3$ solution and (b) film state.

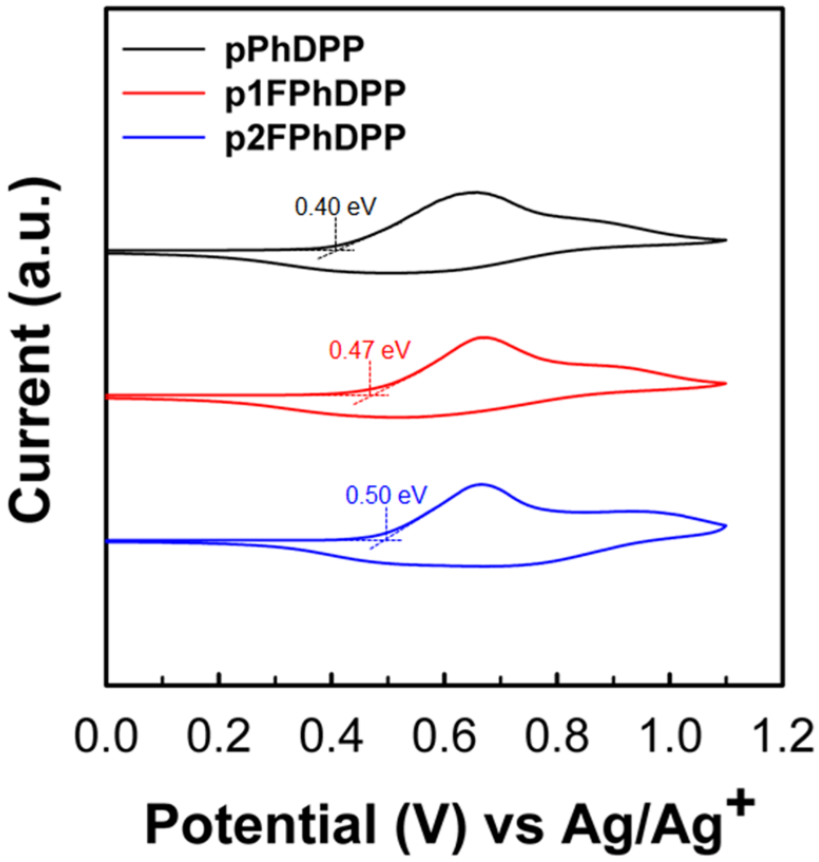

Figure 3.15 Cyclic voltammograms of the polymers.

Table 3.1 Summary of properties of the polymers

Polymer	M_n (kDa)	PDI	λ_{max} (nm)/FWHM (nm)		$E_g^{opt[a]}$ (eV)	E_{HOMO} (eV)	$E_{LUMO}^{[b]}$ (eV)
			Solution	Film			
pPhDPP	98.9	1.43	718/200	674/217	1.48	–5.20	–3.72
p1FPhDPP	126.1	1.37	738/200	682/220	1.44	–5.27	–3.83
p2FPhDPP	127.2	1.40	742/213	693/254	1.41	–5.30	–3.89

[a] is determined from the onset of UV–Vis absorption spectra.

[b] is calculated from the HOMO energy level and the optical bandgap. LUMO = HOMO + E_g^{opt}.

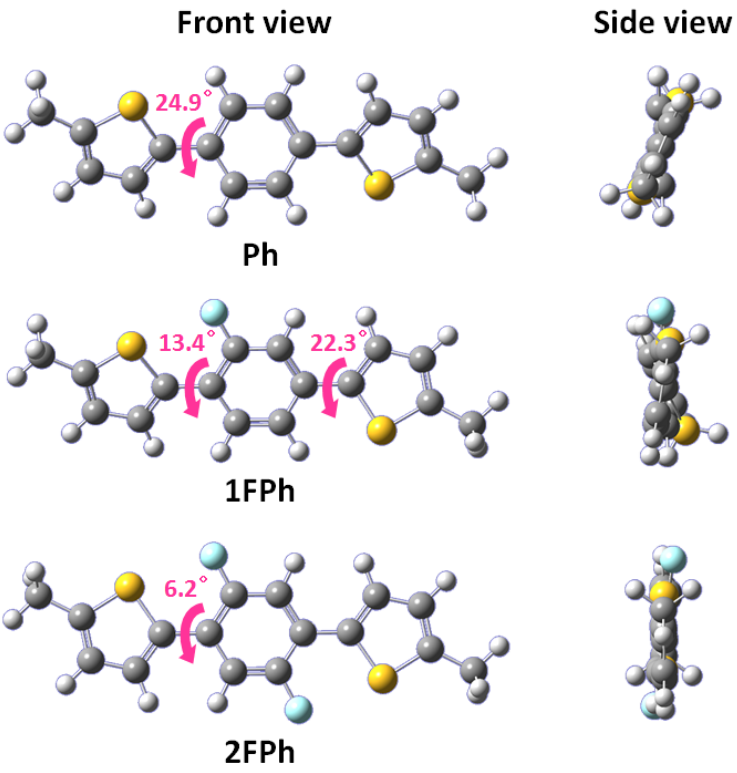

Figure 3.16 Optimized geometry of electron-donating units as determined by the DFT calculation at B3LYP/6-31G(d,p) level

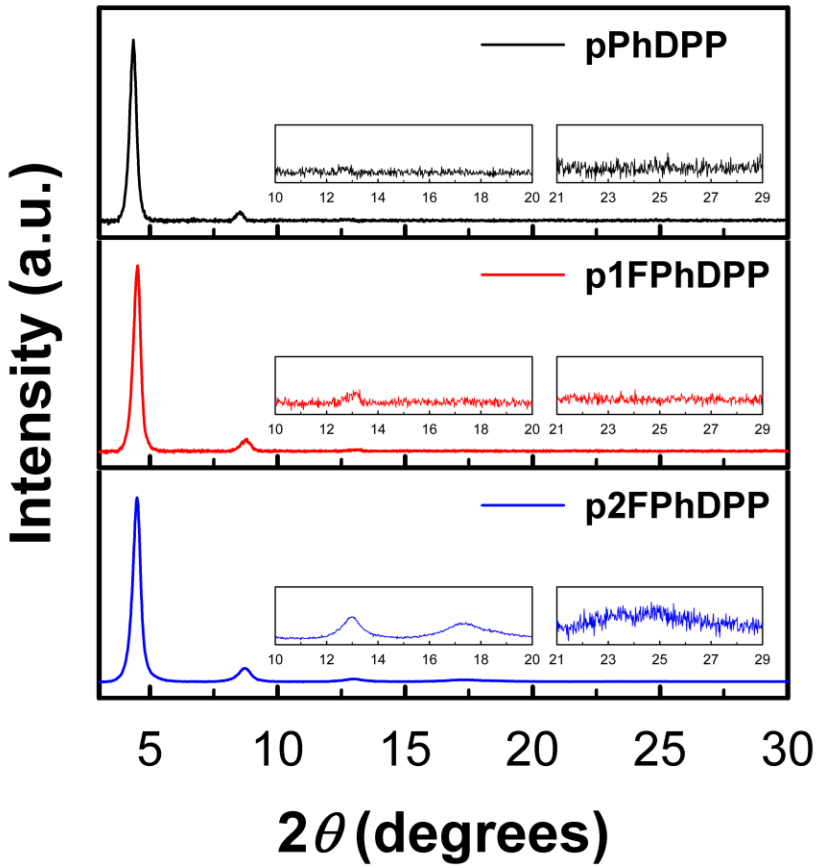

Figure 3.17 X-ray diffraction (XRD) patterns of the polymers.

3.5. Photovoltaic properties

The photovoltaic properties of solar cells were measured with the standard device configuration of ITO/PEDOT:PSS/polymer:$PC_{71}BM$/Ca/Al under one sun illumination (AM 1.5G, 100 mW cm^{-2}). The current density–voltage (*J–V*) curves of the best photovoltaic performance are shown in Figure 3.18. The *J–V* characteristics of photovoltaic devices prepared from polymer:$PC_{71}BM$ of different blend ratio using various solvents and additive are represented in Figure 3.19–21, and photovoltaic parameters are listed in Table 3.2–3.

Since V_{OC} is linearly dependent on the difference between the HOMO energy level of the polymer and the LUMO energy level of the $PC_{71}BM$, the V_{OC}s of fluorinated polymers (0.68 V for p1FPhDPP and 0.72 V for p2FPhDPP) with deeper HOMO levels were higher than that of non-fluorinated polymer (0.59 V for pPhDPP). The J_{SC} is shown as 10.2 mA cm^{-2} for pPhDPP, 11.8 mA cm^{-2} for p1FPhDPP and 12.4 mA cm^{-2} for p2FPhDPP. The J_{SC}s calculated from integration of external quantum efficiency (EQE) spectra are consistent with the J_{SC}s determined from *J–V* curves (Figure 3.22). The fill factor (FF) of pPhDPP, p1FPhDPP and p2FPhDPP is 0.52, 0.58 and 0.63, respectively. The high fill factor of p2FPhDPP could be related to the high charge carrier mobility. As a consequence, the p2FPhDPP-based device exhibits the highest power conversion efficiency of 5.63% with a J_{SC} of 12.4 mA cm^{-2} and a fill factor (FF) of 0.63.

3.6. Charge transport characteristics

The hole mobility have a great impact on charge transport because it is lower than electron mobility, which makes accumulation of electrons, resulting in increasing the probability of bimolecular recombination.[39, 40] Therefore, balanced electron and hole carrier mobility enhances the charge transport ability in solar cell devices. The hole carrier mobility of polymer:$PC_{71}BM$ blend films were measured by the space charge limited current (SCLC) hole mobility measurement. The SCLC hole mobilities can be measured by the standard methods. The single-carrier mobility can be extracted from the dark current density-voltage (J_D–V) curve and is calculated by the trap-free space charge limited current model at low reverse applied voltage using the Mott-Gurney square law. Then, the mobility is obtained from the slope of plot of $J^{1/2}$ *vs*. V_a-V_{bi} (Figure 3. 23), where V_a is the applied potential and V_{bi} is the built-in potential which results from the difference in the work function of the anode and the cathode. The active layers were spin-coated under the conditions that afford the best photovoltaic results. As listed in Table 3.4, the hole mobilities from pPhDPP:$PC_{71}BM$, p1FPhDPP:$PC_{71}BM$ and p2FPhDPP:$PC_{71}BM$ blend films were 9.1 $\times 10^{-5}$ $cm^2/V \cdot s$, 3.3 $\times 10^{-4}$ $cm^2/V \cdot s$ and 7.8 $\times 10^{-4}$ $cm^2/V \cdot s$, respectively. The SCLC hole mobilities of fluorinated polymers are higher than that of non-fluorinated polymer. The higher hole mobilities of fluorinated polymers contribute to higher J_{SC} and higher FF than the values of non-fluorinated polymer

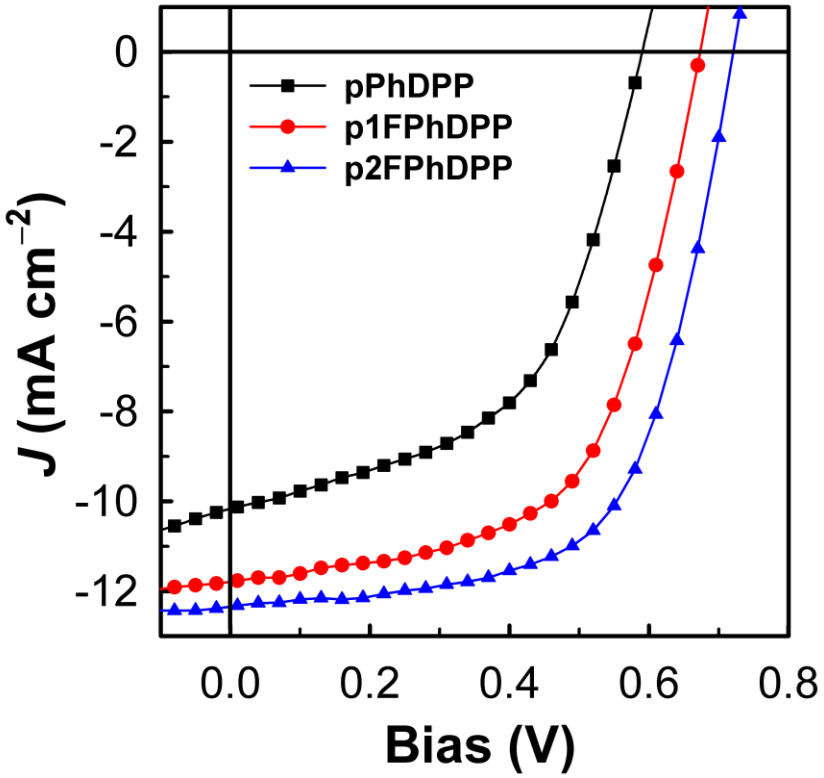

Figure 3.18 Optimized current-voltage (*J*-*V*) characteristics of polymer:$PC_{71}BM$ BHJ solar cells under AM 1.5 condition.

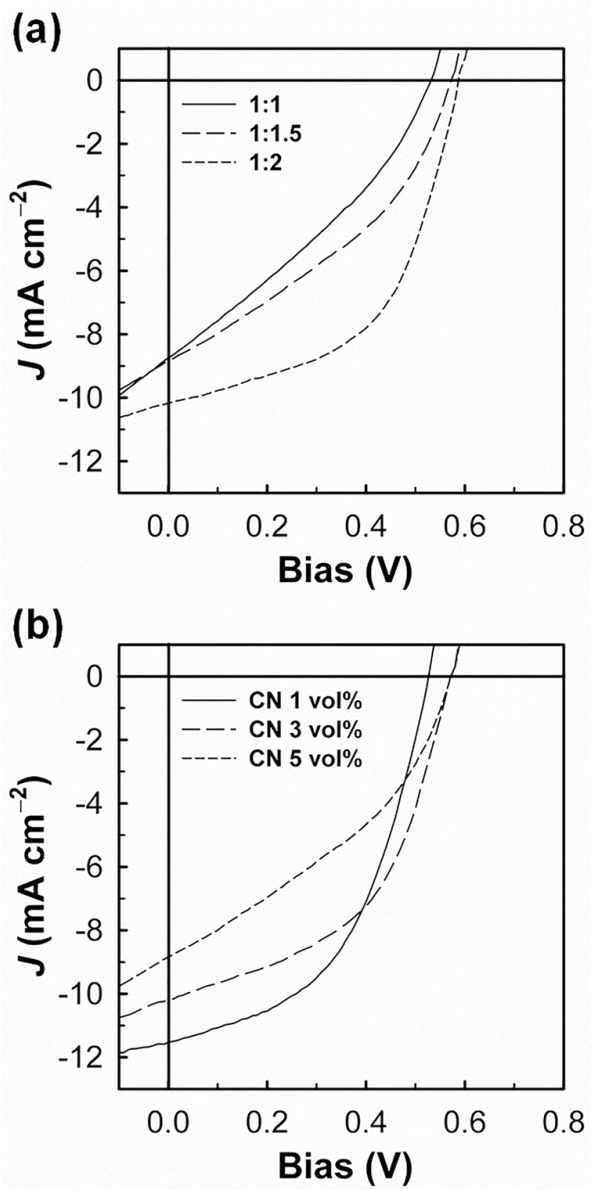

Figure 3.19 *J*–*V* curves of (a) pPhDPP:$PC_{71}BM$ solar cells with different blend ratio and (b) pPhDPP:$PC_{71}BM$ (1:2 w/w) solar cells with different content ratio of 1-chloronaphtalene (CN).

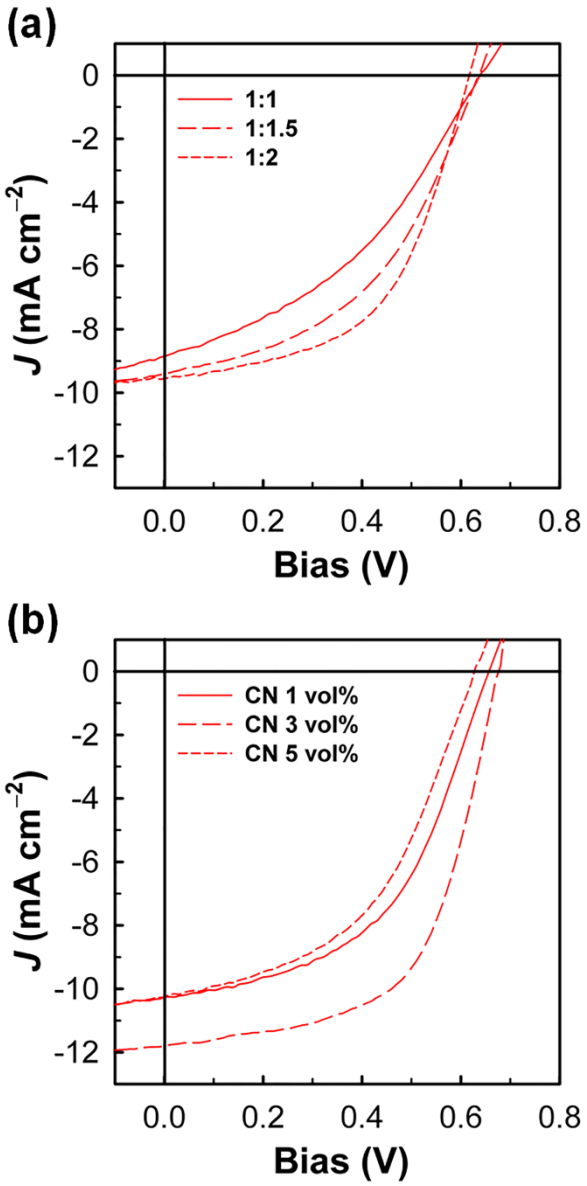

Figure 3.20 *J*–*V* curves of (a) p1FPhDPP:$PC_{71}BM$ solar cells with different blend ratio and (b) p1FPhDPP:$PC_{71}BM$ (1:2 w/w) solar cells with different content ratio of 1-chloronaphtalene (CN).

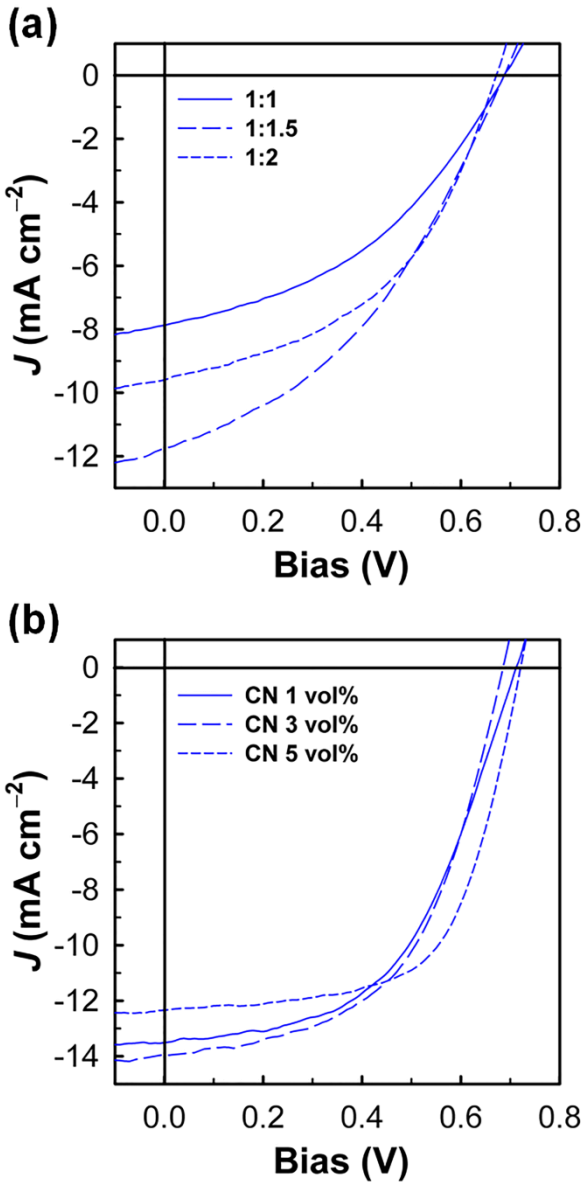

Figure 3.21 *J*–*V* curves of (a) p2FPhDPP:$PC_{71}BM$ solar cells with different blend ratio and (b) p2FPhDPP:$PC_{71}BM$ (1:1.5 w/w) solar cells with different content ratio of 1-chloronaphtalene (CN).

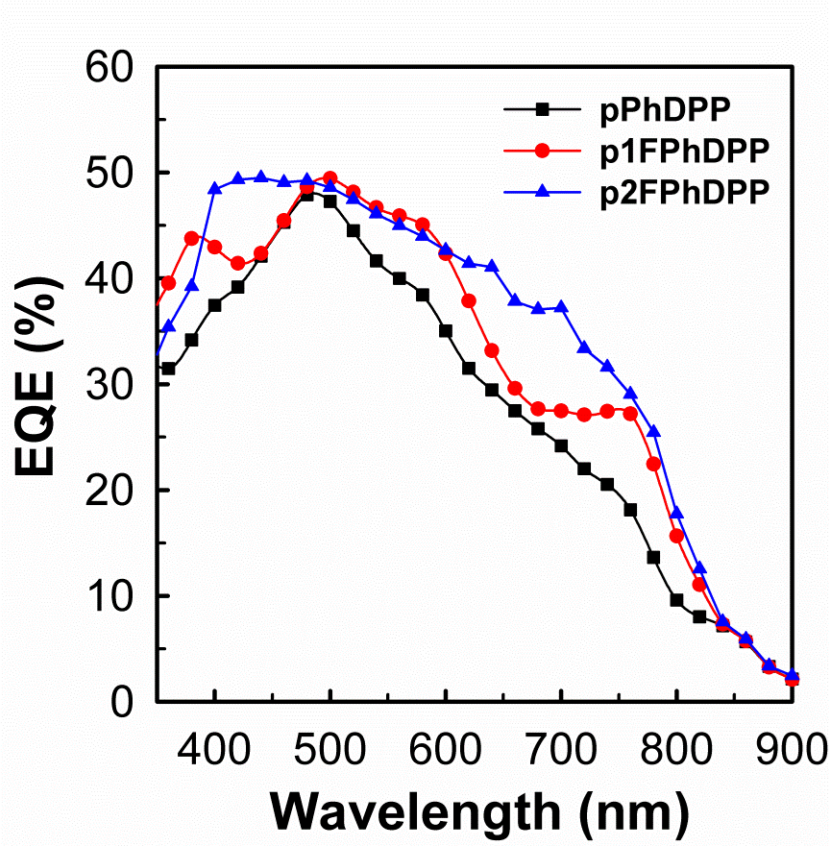

Figure 3.22 External quantum efficiency (EQE) curves of the polymer: $PC_{71}BM$ blend.

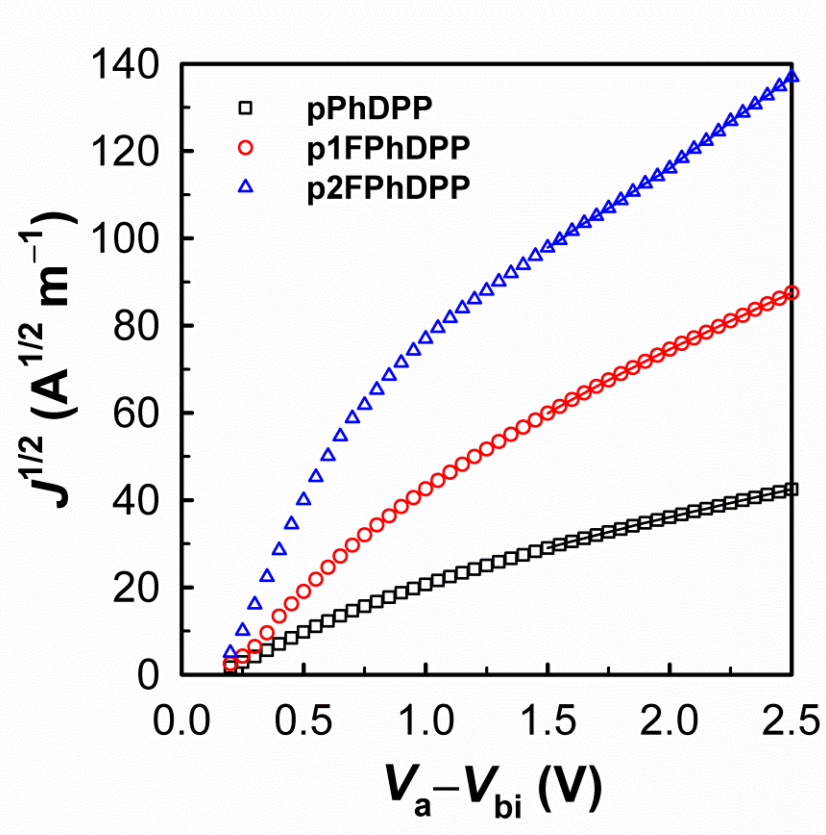

Figure 3.23 Dark *J*–*V* characteristics of polymer:$PC_{71}BM$ with hole-only devices.

Table 3.2 Photovoltaic performances of polymers with different blend ratio of $PC_{71}BM$ under standard AM 1.5G condition

Polymer	Solvent	Blend ratio (w/w)	V_{OC} (V)	J_{SC} (mA cm^{-2})	FF	PCE_{max}(aver) (%)
pPhDPP	DCB	1:1	0.53	8.74	0.32	1.48(1.36)
		1:1.5	0.57	8.84	0.37	1.88(1.75)
		1:2	0.59	10.2	0.52	3.15(3.00)
p1FPhDPP	DCB	1:1	0.64	8.86	0.39	2.21(2.09)
		1:1.5	0.64	9.41	0.45	2.74(2.60)
		1:2	0.62	9.56	0.53	3.15(3.01)
p2FPhDPP	DCB	1:1	0.69	7.88	0.41	2.23(2.10)
		1:1.5	0.69	11.75	0.39	3.18(3.04)
		1:2	0.67	9.60	0.46	2.96(2.79)

Table 3.3 Photovoltaic performances of polymer:$PC_{71}BM$ with different solvent tested under standard AM 1.5G condition

Polymer	Blend ratio (w/w)	Solvent	V_{OC} (V)	J_{SC} (mA cm^{-2})	FF	PCE_{max}(aver) (%)
pPhDPP	1:2	DCB+CN 1 vol%	0.53	11.5	0.49	3.00(2.85)
		DCB+CN 3 vol%	0.58	10.2	0.50	2.96(2.83)
		DCB+CN 5 vol%	0.57	8.8	0.37	1.88(1.75)
p1FPhDPP	1:2	DCB+CN 1 vol%	0.66	10.3	0.50	3.38(3.24)
		DCB+CN 3 vol%	0.68	11.8	0.58	4.65(4.50)
		DCB+CN 5 vol%	0.63	10.3	0.48	3.09(2.88)
p2FPhDPP	1:1.5	DCB+CN 1 vol%	0.71	13.5	0.52	4.98(4.79)
		DCB+CN 3 vol%	0.69	13.9	0.53	5.15(4.96)
		DCB+CN 5 vol%	0.72	12.4	0.63	5.63(5.45)

Table 3.4 Best photovoltaic performances of polymers with $PC_{71}BM$ tested under standard AM 1.5G condition

Polymer	Thickness (nm)	V_{OC} (V)	J_{SC} (mA cm^{-2})	FF	$PCE_{max}(_{aver})$ (%)	Hole mobility[a] ($cm^2V^{-1}s^{-1}$)
pPhDPP	110	0.59	10.2	0.52	3.15(3.00)	9.1×10^{-5}
p1FPhDPP	105	0.68	11.8	0.58	4.65(4.50)	3.3×10^{-4}
p2FPhDPP	110	0.72	12.4	0.63	5.63(5.45)	7.8×10^{-4}

[a] is measured by space-charge limited current methods.

3.7. Morphology investigation

The morphologies of pPhDPP:$PC_{71}BM$, p1FPhDPP:$PC_{71}BM$ and p2FPhDPP:$PC_{71}BM$ blend films were studied using transmission electron microscopy (TEM). The dark regions in the TEM image can be attributed to $PC_{71}BM$ domains due to its relatively high electron scattering density and the bright regions can be attributed to polymer domains.[45] When the morphologies of active layers are examined by TEM, as shown in Figure 3.24. In the blends of pPhDPP:$PC_{71}BM$ blend as shown in Figure 3.24 (a), the phase separation is more coarse and interconnected network is not formed. This will reduce formation of charges, because excitons that are created in the middle of these aggregates need to diffuse over a longer distance to reach the interface with the fullerene phase, where they can dissociate and produce charges. However, for p1FPhDPP and p2FPhDPP with $PC_{71}BM$, the photoactive layers reveal a fibrillar structure in the blend films as shown in Figure 3.24 (b, c), which shows well-interconnected network. The fibrils of p2FPhDPP:$PC_{71}BM$ blend have a width of around 10 nm, which is similar to the exciton diffusion length in conjugated polymers and would allow for efficient dissociation of excitons into electrons and holes. In short, fluorinated polymer-blend films exhibit finer fibrils than mono- and non-fluorinated-blend one, contributing to higher J_{SC}s of fluorinated polymer solar cells than that of mono- and non-fluorinated polymer based solar cell.

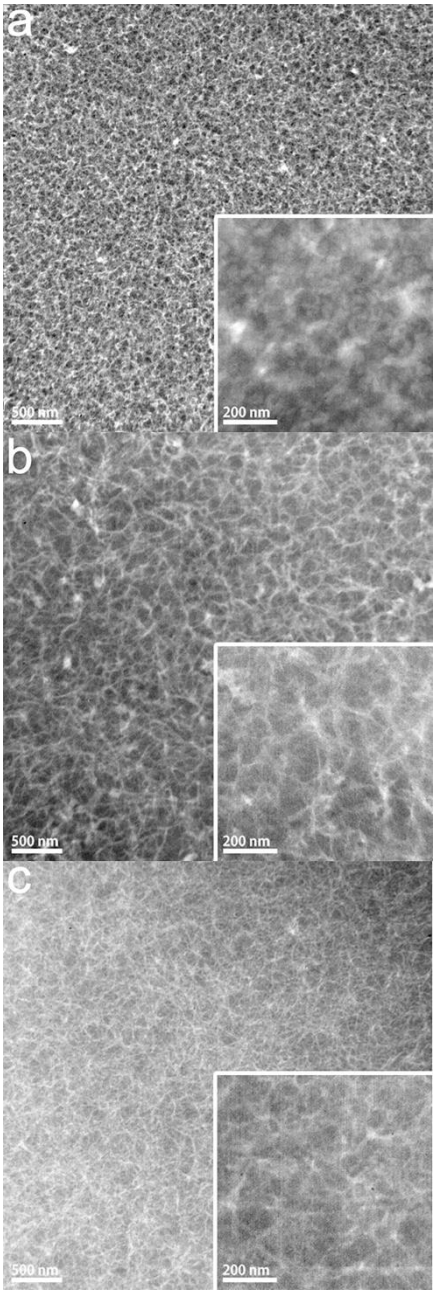

Figure 3.24 TEM images of polymer:$PC_{71}BM$ blends: (a) pPhDPP, (b) p1FPhDPP and (c) p2FPhDPP.

4. Conclusions

In this study, we designed and synthesized DPP-based copolymer with/without fluorine substitution on electron-donating unit (benzene). Compared to non-fluorinated polymer, fluorination on conjugated semiconducting polymer backbone leads to deeper HOMO energy level of polymer and also enhances molecular packing of polymers. The two fluorine substituted polymer (p2FPhDPP) shows deeper HOMO energy level, closer packing due to chain planarity, higher SCLC hole mobility due to effective π–π stacking, and finer fibril morphology than mono- and non-substituted polymers, exhibiting the highest PCE of 5.63% with a V_{OC} of 0.72 V, a J_{SC} of 12.4 mA cm^{-2} and a FF of 0.63. In short, the fluorination on electron-donating unit in D–A type copolymer may provide an effective strategy to achieve high performance polymer solar cells.

Bibliography

(1) Krebs, F. C., *Polymer Photovoltaics A Practical Approach*, SPIE Press, Bellingham, **2008**.

(2) Brabec, C. J.; Sariciftci, N. S.; Hummelen, J. C., *Adv. Funct. Mater.* **2001**, *11*, 15.

(3) Coakley, K. M.; McGehee, M.D., *Chem. Mater.*, **2004**, *16*, 4533.

(4) Cheng, Y. J.; Yang, S.H.; Hsu, C.S., *Chem. Rev.*, **2009**, *109*, 5868.

(5) You, J.; Dou, L.; Yoshimura, K.; Kato, T.; Ohya, K.; Moriarty, T., *Nat. Commun.* **2013**, *4*, 1446.

(6) Dou, L.; Chang, W.-H.; Gao, J.; Chen, C.-C.; You, J.; Yang, Y., *Adv. Mater.* **2013**, *25*, 825.

(7) He, Z.; Zhong, C.; Su, S.; Xu, M.; Wu, H.; Cao, Y., *Nat. Photonics* **2012**, *6*, 593.

(8) Li, W.; Furlan, A.; Hendriks, K.; Wienk, M.; Janssen, R.A.J., *J. Am. Chem. Soc.* **2013**, *135*, 5529.

(9) You, J.; Chen, C.-C.; Hong, Z.; Yoshimura, K.; Ohya, K.; Xu, R., *Adv. Mater.* **2013**, *25*, 3973.

(10) Hoppe, H.; Sariciftci, N. S. J., *Mater. Res.* **2004**, *19*, 1924.

(11) Thompson, B. C.; Frechet, J. M. J., *Angew. Chem., Int. Ed.* **2008**, *47*, 58.

(12) Muntwiler, M.; Yang, Q.; Tisdale, W. A.; Zhu, X. Y., *Phys. Rev. Lett.*, **2008**, *101*, 196403.

(13) Bittner, E. R.; Santos, R. J. G.; Karabunarliev, S., *J. Chem. Phys.*, **2005**, *122*, 214719.

(14) Gledhill, S. E.; Scott, B.; Gregg, B. A., *J. Mater. Res*., **2005**, *20*, 3167.

(15) Liang, Y.; Xu, Z.; Xia, J.; Tsai, S.-T.; Wu, Y.; Li, G.; Ray, C.; Yu, L., *Adv. Mater.* **2010**, *22*, E135.

(16) Zhou, H. X.; Yang, L. Q.; Stuart, A. C.; Price, S. C.; Liu, S. B.; You, W., *Angew. Chem., Int. Ed.* **2011**, *50*, 2995.

(17) Son, H. J.; Wang, W.; Xu, T.; Liang, Y.; Wu, Y.; Li, G.; Yu, L., *J. Am. Chem. Soc.* **2011**, *133*, 1885.

(18) Dou, L.; You, J.; Yang, J.; Chen, C.-C.; He, Y.; Murase, S.; Moriarty, T.; Emery, K.; Li, G.; Yang, Y., *Nat. Photon.* **2012**, *6*, 180.

(19) Gendron, D.; Leclerc, M., New conjugated polymers for plastic solar cells. *Energy Environ. Sci.* **2011**, *4*, 1225.

(20) Chochos, C. L.; Choulis, S. A., *Prog. Polym. Sci.* **2011**, *36*, 1326.

(21) Li, Y., *Acc. Chem. Res.* **2012**, *45*, 723.

(22) Boudreault, P.-L. T.; Najari, A.; Leclerc, M., *Chem. Mater.* **2011**, *23*, 456.

(23) Zhou, H. X.; Yang, L. Q.; You, W., *Macromolecules* **2012**, *45*, 607.

(24) He, Z.; Zhong, C.; Huang, X.; Wong, W. Y.; Wu, H.; Chen, L.; Su, S.;

Cao, Y., *Adv. Mater.* **2011**, *23*, 4636.

(25) Jheng, J. F.; Lai, Y. Y.; Wu, J. S.; Chao, Y. H.; Wang, C. L.; Hsu, C. S., *Adv. Mater.* **2013**, *25*, 2445.

(26) Jo, J. W.; Kim, S. S.; Jo, W. H., *Org. Electron.* **2012**, *13*, 1322.

(27) Osaka, I.; Shimawaki, M.; Mori, H.; Doi, I.; Miyazaki, E.; Koganezawa, T.; Takimiya, K., *J. Am. Chem. Soc.* **2012**, *134*, 3498.

(28) Ashraf, R. S.; Schroeder, B. C.; Bronstein, H. A.; Huang, Z.; Thomas, S.; Kline, R. J.; Brabec, C. J.; Rannou, P.; Anthopoulos, T. D.; Durrant, J. R.; McCulloch, I., *Adv. Mater.* **2013**, *25*, 2029.

(29) Dou, L.; Chang, W. H.; Gao, J.; Chen, C. C.; You, J.; Yang, Y., *Adv. Mater.* **2013**, *25*, 825.

(30) Hendriks, K. H.; Heintges, G. H.; Gevaerts, V. S.; Wienk, M. M.; Janssen, R. A., *Angew. Chem. Int. Ed.* **2013**, *52*, 8341.

(31) Li, W.; Furlan, A.; Hendriks, K. H.; Wienk, M. M.; Janssen, R. A., *J. Am. Chem. Soc.* **2013**, *135*, 5529.

(32) Li, Y. N.; Sonar, P.; Murphy, L.; Hong, W., *Energy Environ. Sci.* **2013**, *6*, 1684.

(33) Zoombelt, A. P.; Mathijssen, S. G. J.; Turbiez, M. G. R.; Wienk, M. M.; Janssen, R. A. J., *J. Mater. Chem.* **2010**, *20*, 2240.

(34) Zhou, E. J.; Cong, J. Z.; Hashimoto, K.; Tajima, K., *Energy Environ. Sci.* **2012**, *5*, 9756.

(35) Zhou, H.; Yang, L.; Stuart, A. C.; Price, S. C.; Liu, S.; You, W., *Angew. Chem. Int. Ed.* **2011**, *50*, 2995.

(36) Cheng, Y. J.; Yang, S. H.; Hsu, C. S., *Chem. Rev.* **2009**, *109*, 5868.

(37) Perez, M. D.; Borek, C.; Forrest, S. R.; Thompson, M. E., *J. Am. Chem. Soc.* **2009**, *131*, 9281.

(38) Stuart, A. C.; Tumbleston, J. R.; Zhou, H.; Li, W.; Liu, S.; Ade, H.; You, W., *J. Am. Chem. Soc.* **2013**, *135*, 1806.

(39) Yang, L. Q.; Tumbleston, J. R.; Zhou, H. X.; Ade, H.; You, W., *Energy Environ. Sci.* **2013**, *6*, 316.

(40) Li, W.; Furlan, A.; Roelofs, W. S.; Hendriks, K. H.; van Pruissen, G. W.; Wienk, M. M.; Janssen, R. A., *Chem. Comm.* **2014**, *50*, 679.

(41) Jo, J. W.; Jung, J. W.; Wang, H. W.; Kim, P.; Russell, T. P.; Jo, W. H., *Chem. Mater.* **2014**, *26*, 4214.

(42) Jo, J. W.; Bae, S.; Liu, F.; Russell, T. P.; Jo, W. H., *Adv. Funct. Mater.* **2014**, http://dx.doi.org/10.1002/adfm.201402210.

(43) Son, H. J.; Wang, W.; Xu, T.; Liang, Y.; Wu, Y.; Li, G.; Yu, L., *J. Am. Chem. Soc.* **2011**, *133*, 1885.

(44) Facchetti, A., *Chem. Mater.* **2011**, *23*, 733.

(45) Moon, J.S.; Lee, J.K.; Cho, S.; Byun, J.; Heeger, A.J., *Nano Letters*, **2009**, *9*, 230.

초 록

불소화가 광전지 성능에 미치는 영향을 탐구하기 위해 각각 싸이오펜이 붙은 디케토피롤로피롤과 불소 치환 된 벤젠, 치환 안된 벤젠으로 이루어진 좁은 밴드갭의 고분자가 중합되었다. 벤젠에 치환된 불소 원자의 개수가 많아질수록 고분자의 HOMO와 LUMO 에너지 래벨이 낮아졌으며 결정성은 향상되었다. 또한, 치환된 불소 원자 수가 증가할수록 고분자:$PC_{71}BM$ 혼합물의 필름상태에서 섬유모양 크기가 작아졌다. 그 결과, 두 개의 불소 원자가 치환된 고분자는 –5.30 eV의 낮은 HOMO 에너지 래벨을 보였으며 이로 인해 0.72 V의 높은 개방 전압을 나타내었다. 또, 고분자 사슬의 패킹을 나타내는 결정성의 향상은 불소가 하나 치환된 것과 치환되지 않은 것들과 비교해 12.4 mA cm^{-2}의 높은 단락 전류를 갖는데 선두적인 역할을 하였다. 따라서 불소 원자 두 개가 치환된 고분자를 통해 만든 태양전지는 5.63%의 유망한 동력변환효율을 나타내었다.

주요어: 고분자 태양 전지, 디케토피롤로피롤, 공액 고분자, 불소화
학 번: 2013-22480